

Monolayer polar metals with large piezoelectricity derived from MoSi_2N_4

Yan Yin,[†] Qihua Gong,^{*,†,‡} and Min Yi^{*,†}

[†]*State Key Laboratory of Mechanics and Control for Aerospace Structures & Key Laboratory for Intelligent Nano Materials and Devices of Ministry of Education & Institute for Frontier Science & College of Aerospace Engineering, Nanjing University of Aeronautics and Astronautics (NUAA), Nanjing 210016, China*

[‡]*MIIT Key Laboratory of Aerospace Information Materials and Physics & College of Physics, Nanjing University of Aeronautics and Astronautics (NUAA), Nanjing 211106, China*

E-mail: gongqihua@nuaa.edu.cn; yimin@nuaa.edu.cn

Abstract

The advancement of two-dimensional polar metals tends to be limited by the incompatibility between electric polarity and metallicity as well as dimension reduction. Here, we report polar and metallic Janus monolayers of MoSi_2N_4 family by breaking the out-of-plane (OOP) structural symmetry through Z (P/As) substitution of N. Despite the semiconducting nature of MoSi_2X_4 (X=N/P/As), four Janus $\text{MoSi}_2\text{N}_x\text{Z}_{4-x}$ monolayers are found to be polar metals owing to the weak coupling between the conducting electrons and electric polarity. The metallicity is originated from the Z substitution induced delocalization of occupied electrons in Mo-d orbitals. The OOP electric polarizations around 10–203 pC/m are determined by the asymmetric OOP charge distribution due to the non-centrosymmetric Janus structure. The corresponding OOP piezoelectricity is further revealed as high as 39–153 pC/m and 0.10–0.31 pm/V for piezoelectric

strain and stress coefficients, respectively. The results demonstrate polar metallicity and high OOP piezoelectricity in Janus $\text{MoSi}_2\text{N}_x\text{Z}_{4-x}$ monolayers and open new vistas for exploiting unusual coexisting properties in monolayers derived from MoSi_2N_4 family.

Keywords: 2D MoSi_2N_4 family, Janus $\text{MoSi}_2\text{N}_x\text{Z}_{4-x}$ monolayers, Polar metals, Out-of-plane piezoelectricity, *ab initio* calculations

1. INTRODUCTION

Metals with electric polarization have emerged to exhibit fantastic physical properties, e.g., ferroelectricity, superconductivity and magnetoelectricity.¹⁻⁸ Polar metals are considered as a more appropriate way to define the metals in a polar space group before the polarization switchability remains unresolved.⁹ Several two-dimensional (2D) polar metals have been reported, for instance, the tri-layer superlattices $\text{BaTiO}_3/\text{SrTiO}_3/\text{LaTiO}_3$,⁵ the multiferroic metal $\alpha\text{-In}_2\text{Se}_3$ ¹⁰ and the artificial ferroelectric $\text{Ba}_{0.2}\text{Sr}_{0.8}\text{TiO}_3$ thin films.¹¹ Cobden et al. found that non-polar topological semimetal WTe_2 exhibits spontaneous out-of-plane (OOP) electric polarization and metallicity through two- or three-layer stacking.¹² Recently, a large family of 2D bimetal phosphates have been systematically investigated, including 16 ferroelectric metals.¹³ The ferroelectricity is attributed to the break of spontaneous symmetry induced by the opposite vertical displacements of different bimetal atoms. The previous studies have no doubt revealed the intriguing phenomena in 2D polar metals and boosted the development of other materials. Currently, seeking more 2D polar metals still deserves more efforts and the pace has never stopped.

MoSi_2N_4 is a novel 2D material that has been experimentally synthesized¹⁴ and is further expanded to MA_2Z_4 family in theoretical investigations.¹⁵ In MA_2Z_4 , M is Group IVB – VIB transition-metal elements, A is Si or Ge and Z is Group VA elements (N/P/As). The element

selectivity brings structural diversity of MA_2Z_4 and further renders the family with intriguing chemical and physical properties which have been involved in the fields of electronics, optoelectronics, thermal transport and spintronics.^{15–27} It is found that semiconducting or metallic character of monolayer MA_2Z_4 is dependent on the valence electron counts (VECs) of the system,^{15,28} where the transition-metal atom rather than the structural phase plays a key role. For instance, the majority of MA_2Z_4 with Group IVB or VIB elements (32 or 34 VECs in total) are semiconductors, while those with VB elements (33 VECs in units cell) are metals. However, the influence of structural phase on MA_2Z_4 is rarely examined. Janus MSiGeN_4 ($\text{M} = \text{Mo/W}$) monolayers, are revealed as indirect bandgap semiconductors with a high electron mobility.²⁹ Meanwhile, MSiGeN_4 monolayers have in-plane and OOP polarizations under a uniaxial strain and valley polarization under the spin-orbit coupling. Recently, the transition from Stoner ferromagnetism to half-metal by hole doping in $\text{MoN}_2\text{X}_2\text{Y}_2$ ($\text{X}, \text{Y} = \text{Group IIIA or VIA elements}$) is presented.³⁰ Nevertheless, polar metallic members have so far never been reported in MA_2Z_4 family.

Motivated by the diversity and designability of MA_2Z_4 family, here we design 16 novel $\text{MoSi}_2\text{N}_x\text{Z}_{4-x}$ ($\text{N} = \text{P/As}$) monolayers through Z substitution of N in MoSi_2N_4 by first-principles calculations. 13 $\text{MoSi}_2\text{N}_x\text{Z}_{4-x}$ structures are found stable in terms of formation energy and lattice stability, among which there are 6 semiconductors and 7 metals. Particularly, although MoSi_2X_4 ($\text{X}=\text{N/P/As}$) monolayers are all semiconductors, 4 kinds of Janus $\text{MoSi}_2\text{N}_x\text{Z}_{4-x}$ monolayers with non-centrosymmetry along OOP direction are demonstrated to be polar metals. The metallicity is attributed to the Z substitution induced delocalization of electrons around Mo atoms and thus the obvious honeycomb-like conducting network. The OOP polarization (P_{out}) of these metallic Janus monolayers are predicted as 10–203 pC/m, which are higher than that of most 2D materials. The excellent OOP piezoelectricity of these polar metallic Janus $\text{MoSi}_2\text{N}_x\text{Z}_{4-x}$ monolayers is also expounded, with the piezoelectric strain and stress coefficients around 39–153 pC/m and 0.10–0.31 pm/V, respectively. These results advocate Janus $\text{MoSi}_2\text{N}_x\text{Z}_{4-x}$ monolayers as polar metals with large piezoelec-

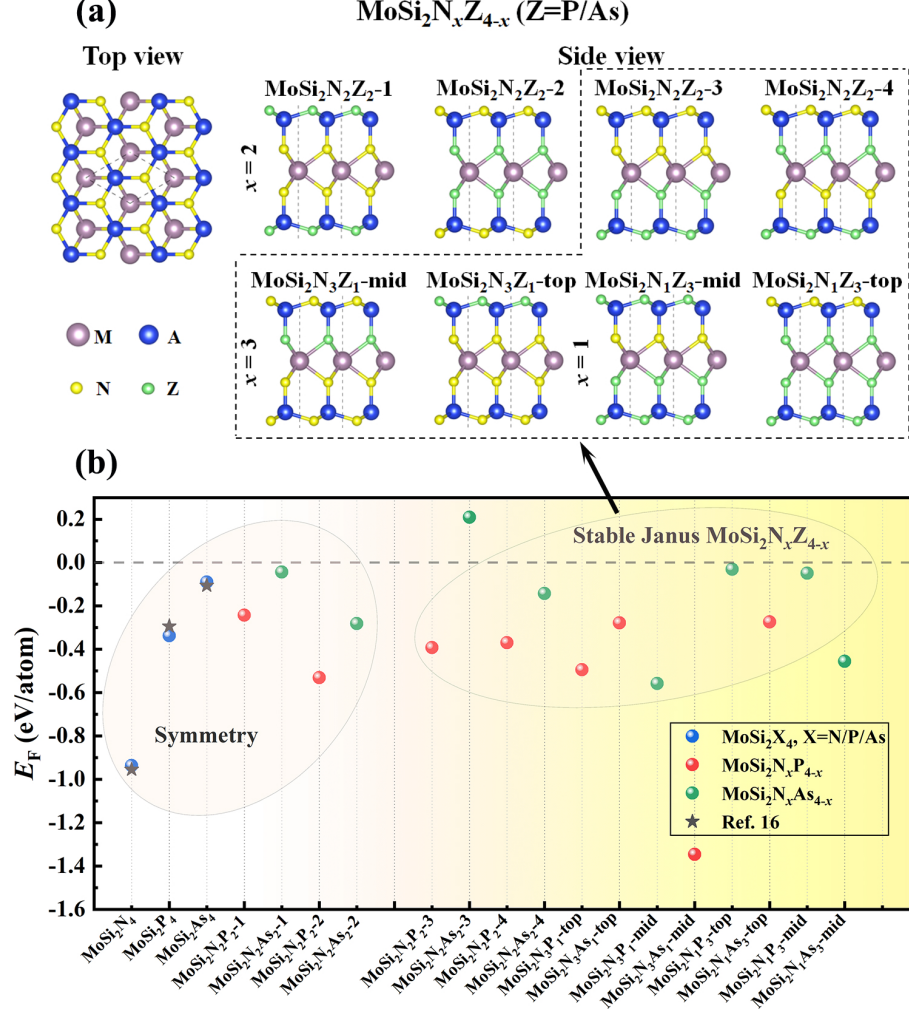


Figure 1: (a) Top and side view of lattice structure. (c) Formation energy (E_F) of MoSi_2X_4 ($\text{X} = \text{N}/\text{P}/\text{As}$) and $\text{MoSi}_2\text{N}_x\text{Z}_{4-x}$ ($x = 1, 2, 3, 4$) monolayers.

tricity, providing new opportunities for realizing 2D multifunctional materials with unusual coexisting properties.

2. RESULTS AND DISCUSSION

2.1. Lattice structure and stability

Monolayer MoSi_2N_4 , a 7-atomic-layer structure with a hexagonal unit cell, is built by intercalating a 2H- MoS_2 -type MoN_2 layer into an α - InSe -type Si_2N_2 . It can be also considered as a structure with mirror symmetry centred on Mo atom. Four N atomic layers locate at

the two side of Mo layer, and Si atoms bridge N atoms from the side view. Here, after substituting N with P/As atoms, monolayer $\text{MoSi}_2\text{N}_x\text{Z}_{4-x}$ ($x = 1, 2, 3, 4$) possesses the similar configuration, as shown in Fig. 1(a). Four layers of Z ($\text{Z} = \text{P/As}$) atoms are alternated with Mo and Si layers, resulting in 18 kinds of lattice structures. The corresponding substitution ratio (R_s) for N is 0% (reference phase MoSi_2N_4), 25% ($\text{MoSi}_2\text{N}_3\text{Z}_{1\text{-mid}}$, $\text{MoSi}_2\text{N}_3\text{Z}_{1\text{-top}}$), 50% ($\text{MoSi}_2\text{N}_2\text{Z}_{2\text{-1}}$, $\text{MoSi}_2\text{N}_2\text{Z}_{2\text{-2}}$, $\text{MoSi}_2\text{N}_2\text{Z}_{2\text{-3}}$, $\text{MoSi}_2\text{N}_2\text{Z}_{2\text{-4}}$), 75% ($\text{MoSi}_2\text{N}_3\text{Z}_{1\text{-mid}}$, $\text{MoSi}_2\text{N}_3\text{Z}_{1\text{-top}}$) and 100% (previously reported MoSi_2P_4 and MoSi_2As_4 ¹⁵). When $R_s = 0$ or 100%, the lattice belongs to the space group of $P\bar{6}m2$ (No. 187) and shows “high-symmetry phase”. With Z atoms substitution, four types ($\text{MoSi}_2\text{N}_2\text{P}_{2\text{-1}}$, $\text{MoSi}_2\text{N}_2\text{P}_{2\text{-2}}$, $\text{MoSi}_2\text{N}_2\text{As}_{2\text{-1}}$, and $\text{MoSi}_2\text{N}_2\text{As}_{2\text{-2}}$) remain this mirror symmetry. Since the reduction of spontaneous geometric symmetry, other 12 structures with different Z atoms are subordinate to $P3m1$ (No. 156) group. The determined lattice parameters are listed in Table S1. One can find that in pure MoSi_2X_4 the lattice constants, effective thickness (h) and bond lengths increase with the increasing period number of elements Z from N, P to As. The similar phenomenon also occurs in $\text{MoSi}_2\text{N}_x\text{Z}_{4-x}$ and is more notable when Z (P/As) locates at the outermost side.

Then, we explore the stability of monolayer $\text{MoSi}_2\text{N}_x\text{Z}_{4-x}$. The formation energy (E_F) of $\text{MoSi}_2\text{N}_x\text{Z}_{4-x}$ is summarized in Fig. 1(b) and Table S1. E_F of MoSi_2N_4 , MoSi_2P_4 and MoSi_2As_4 are -0.94, -0.34 and -0.09 eV/atom, respectively, agreeing well with the previous reports.¹⁵ The negative E_F demonstrates the exothermic reaction and the possibility of experimental existence. Thus, 15 $\text{MoSi}_2\text{N}_x\text{Z}_{4-x}$ monolayers with negative E_F are energetically stable and only one ($\text{MoSi}_2\text{N}_2\text{As}_{2\text{-3}}$) with positive E_F is unstable. On the other hand, the phonon dispersion spectra of $\text{MoSi}_2\text{N}_x\text{Z}_{4-x}$ (Fig. S1 and S2) show that 13 $\text{MoSi}_2\text{N}_x\text{Z}_{4-x}$ and 3 MoSi_2X_4 ($\text{X}=\text{N/P/As}$) monolayers without imaginary frequency are dynamically stable. Therefore, in addition to MoSi_2X_4 , $\text{MoSi}_2\text{N}_x\text{Z}_{4-x}$ monolayers are predicted as new and stable counterparts that are derived from MoSi_2N_4 in terms of formation energy and lattice dynamics. Meanwhile, there are 9 kinds of Janus $\text{MoSi}_2\text{N}_x\text{Z}_{4-x}$ monolayers as shown in Fig. 1(b)

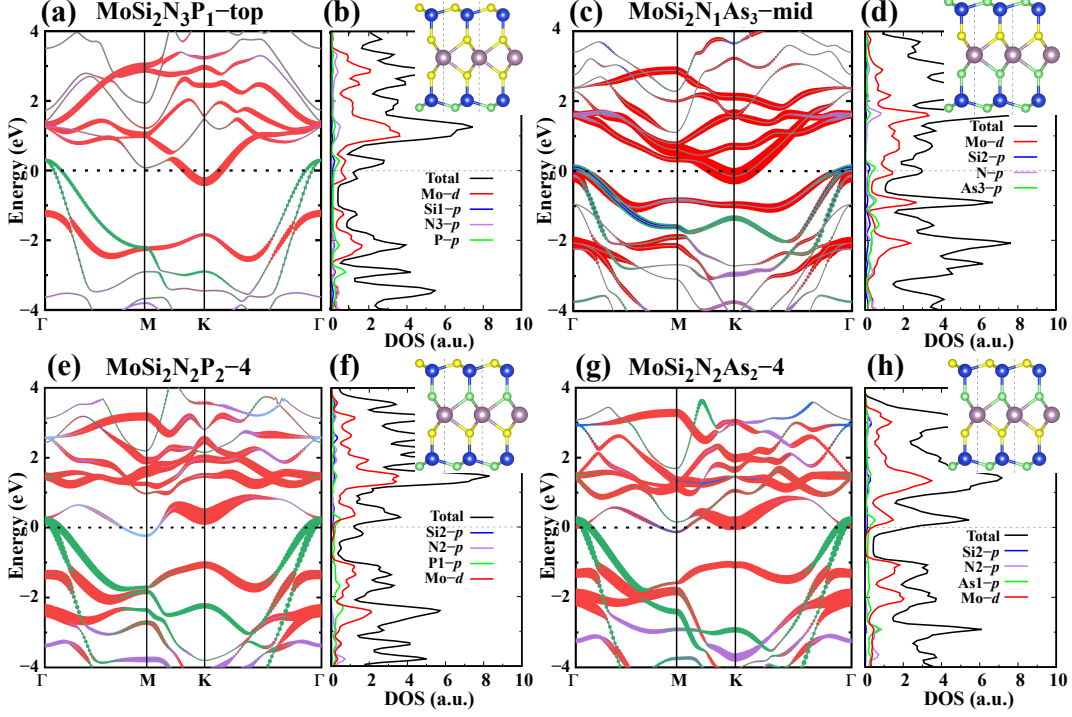


Figure 2: Band structure and DOS of (a) (b) $\text{MoSi}_2\text{N}_3\text{P}_1\text{-top}$, (c) (d) $\text{MoSi}_2\text{N}_1\text{As}_3\text{-mid}$, (e) (f) $\text{MoSi}_2\text{N}_2\text{P}_2\text{-4}$, (g) (h) $\text{MoSi}_2\text{N}_2\text{As}_2\text{-4}$. The dot lines at zero energy represent the Fermi level.

and Table S1.

2.2 Metallic Janus $\text{MoSi}_2\text{N}_x\text{Z}_{4-x}$ monolayers

The electric properties of Janus $\text{MoSi}_2\text{N}_x\text{Z}_{4-x}$ monolayers are firstly investigated via band structure (Figs. S4). Three MoSi_2X_4 semiconductors exhibit decreasing band gap from N, P to As (Fig. S3), which are in good agreement with previous calculations.^{15,22} This manifests that the band gap of MoSi_2Z_4 reduces with the increasing atomic period in the same group. For other 13 stable $\text{MoSi}_2\text{N}_x\text{Z}_{4-x}$ monolayers, 6 are semiconductors with the band gap of 0.01–0.54 eV for PBE and 0.40–0.96 eV for HSE06 functional (Table S1 and Fig. S4). However, the band gap has no dependence on the lattice constant of $\text{MoSi}_2\text{N}_x\text{Z}_{4-x}$, which is different from MoSi_2X_4 and A-site-substituted $\text{MoN}_2\text{X}_2\text{Y}_2$.³⁰ Additionally, there exist 7 metals in $\text{MoSi}_2\text{N}_x\text{Z}_{4-x}$ monolayer, i.e., $\text{MoSi}_2\text{N}_3\text{P}_1\text{-top}$, $\text{MoSi}_2\text{N}_2\text{P}_2\text{-1}$, $\text{MoSi}_2\text{N}_2\text{P}_2\text{-4}$, $\text{MoSi}_2\text{N}_2\text{As}_2\text{-1}$, $\text{MoSi}_2\text{N}_2\text{As}_2\text{-2}$, $\text{MoSi}_2\text{N}_2\text{As}_2\text{-4}$ and $\text{MoSi}_2\text{N}_1\text{As}_3\text{-mid}$. Among them, there are 4 metals with

Janus structure, as shown in Fig. 2.

To reveal the origin of metallic properties in $\text{MoSi}_2\text{N}_x\text{Z}_{4-x}$, we examine the projected band structure and density of states (DOS) of four Janus monolayers (Fig. 2), i.e., $\text{MoSi}_2\text{N}_3\text{P}_1$ -top, $\text{MoSi}_2\text{N}_2\text{P}_2$ -4, $\text{MoSi}_2\text{N}_2\text{As}_2$ -4, and $\text{MoSi}_2\text{N}_1\text{As}_3$ -mid, which contains various substitution ratios and different OOP non-centrosymmetric structures. Firstly, these four monolayers are all metals with three energy bands crossing Fermi level, which are the 16th, 17th and 18th band. From the partial DOS, it is found that these energy bands near the Fermi level are mainly occupied by electrons from Mo-*d* orbitals in $\text{MoSi}_2\text{N}_x\text{Z}_{4-x}$, especially near the high-symmetry point of K. There also exists a little contribution from the *p*-orbital electrons of outermost P/As atoms on the side where N bridges Si and Mo. Secondly, $\text{MoSi}_2\text{N}_2\text{P}_2$ -4 and $\text{MoSi}_2\text{N}_2\text{As}_2$ -4 exhibit the same structural configuration (Z-Si-N-Mo-Z-Si-N) and thus the similar band structures, as shown in Fig. 2 (e)–(h)). Actually, other $\text{MoSi}_2\text{N}_x\text{Z}_{4-x}$ monolayers with the same structural configuration show the similar energy bands as well (Fig. S4). The electronic properties of different $\text{MoSi}_2\text{N}_x\text{Z}_{4-x}$ monolayers, however, are different. For instance, $\text{MoSi}_2\text{N}_2\text{P}_2$ -2 and $\text{MoSi}_2\text{N}_2\text{P}_2$ -3 are semiconductors, whereas $\text{MoSi}_2\text{N}_2\text{As}_2$ -2 and $\text{MoSi}_2\text{N}_2\text{As}_2$ -3 are metals. The similar energy bands reflect not only the similar effect of Z atoms on electronic properties in $\text{MoSi}_2\text{N}_x\text{Z}_{4-x}$, but also the ability of P/As atoms to reduce the band gap. Thirdly, in centrosymmetric MoSi_2N_4 , the middle plane where Mo atom locates perpendicularly bisects the structure and results in the symmetric distribution of charges. However, the four metallic Janus structures are non-centrosymmetric, implying that there would exist intriguing phenomena caused by the OOP asymmetric charge distribution.

In order to further anatomize the electronic properties of the four Janus metals, we calculate the planar-average charge density along the OOP direction and the charge distribution of three energy bands crossing Fermi level in the real space, as shown in Fig. 3(a)–(d). The planar-average charge density distribution is found to be asymmetric with respect to the (001) plane where Mo atoms are located. From the partial charge density of 16th, 17th,

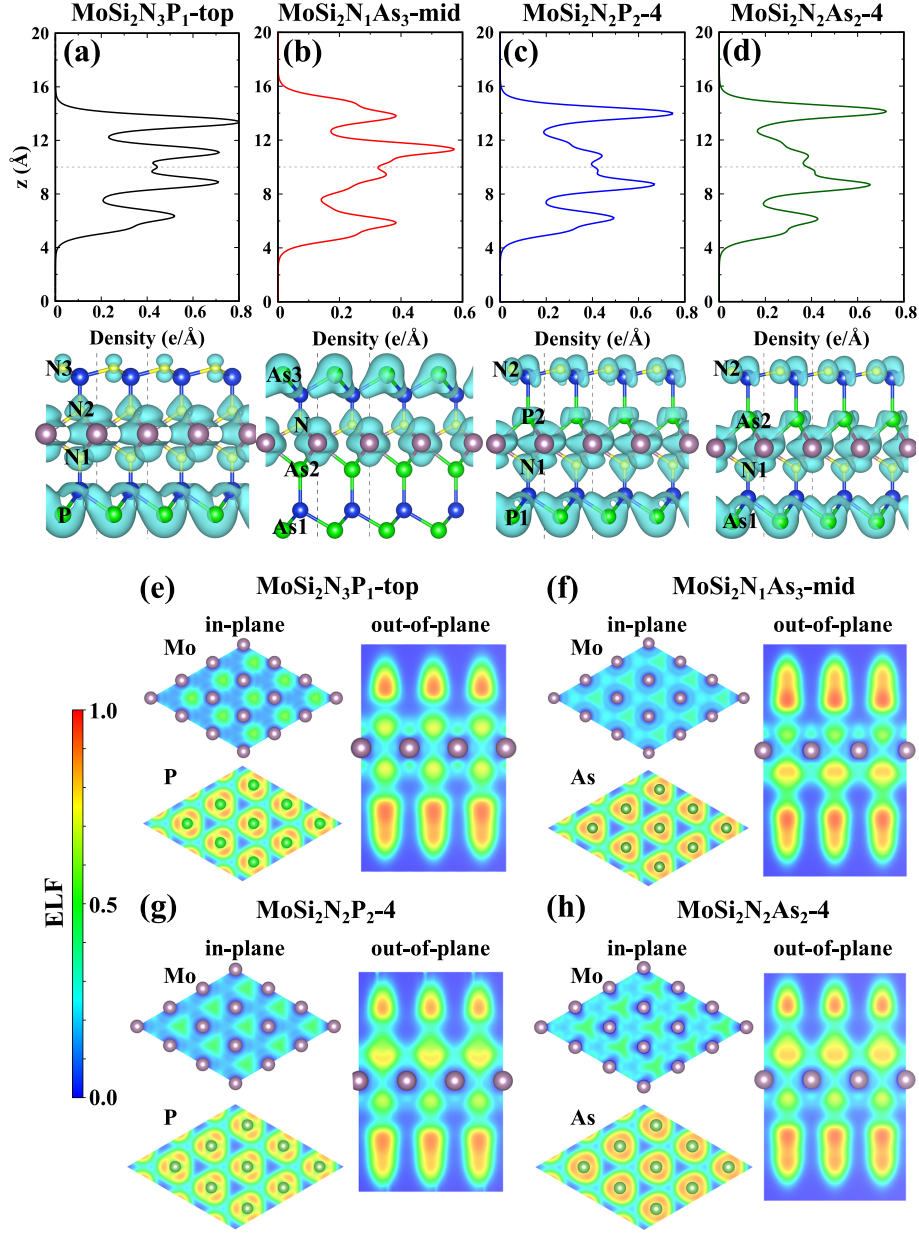


Figure 3: Planar-average charge density along z -direction and partial charge density of the 16th, 17th, and 18th bands in the real place of four metal Janus monolayers: (a) $\text{MoSi}_2\text{N}_3\text{P}_1$ -top, (b) $\text{MoSi}_2\text{N}_1\text{As}_3$ -mid, (c) $\text{MoSi}_2\text{N}_2\text{P}_2$ -4, (d) $\text{MoSi}_2\text{N}_2\text{As}_2$ -4. The isovalue for charge density is $0.02 \text{ e}/\text{\AA}^3$. (e)–(h) Electron localization function (ELF) of in-plane (100) slice and out-of-plane (001) slice.

18th energy bands in Fig. 3(a)–(d), it can be found that the charge distribution are mainly around Mo atoms and the outermost P/As atoms on the side where N bridges Si and Mo, in accordance with the band structure and DOS results in Fig. 2. We further examine the electron localization function (ELF) that could qualitatively describe the strength of electron localization, as shown in Fig. 3(e)–(h). In all these four Janus monolayers, the in-plane ELF crossing Mo atom is about 0.5, indicating the electrons around Mo atom are strongly delocalized. In contrast, ELF crossing P/As atoms is close to 1.0 and thus the electrons around P/As atoms are localized. The electron localization of outermost P/As atoms is related to the strong covalent-like Si-P and Si-As bond. Therefore, the metallicity of these four Janus monolayers could be ascribed to the delocalization nature of electrons around Mo atom.³¹ Specially, in $\text{MoSi}_2\text{N}_1\text{As}_3\text{-mid}$, the delocalized electrons even connect together to form an honeycomb-like conducting network.

2.3 Polar metal and piezoelectricity

In Table 1, the absolute values of P_{out} of Janus monolayer $\text{MoSi}_2\text{N}_3\text{P}_1\text{-top}$, $\text{MoSi}_2\text{N}_1\text{As}_3\text{-mid}$, $\text{MoSi}_2\text{N}_2\text{P}_2\text{-4}$, and $\text{MoSi}_2\text{N}_2\text{As}_2\text{-4}$ are 203, 22, 24, and 10 pC/m, respectively, which are more than ten folds higher than that of many 2D monolayer semiconductors (e.g., MXenes with $P_{\text{out}} = (3\text{--}17)$ pC/m,³² group IVA 2D binary ferroelectric compounds with $P_{\text{out}} = (1\text{--}4)$ pC/m,³³ and defective In_2Se_3 with $P_{\text{out}} = (1\text{--}4)$ pC/m³⁴) and 2D metals (e.g., 2D bimetal phosphates with $P_{\text{out}} = (1\text{--}10)$ pC/m¹³ and Co_2Se_3 with 4 pC/m³⁵), as summarized in Fig. 4(a). The OOP polarization direction (insert figures in Fig. S5) of four Janus metallic $\text{MoSi}_2\text{N}_x\text{Z}_{4-x}$ monolayers points to the out-of-plane direction, to the outermost P/As (on the side where N atom bridges Si and Mo). Such high P_{out} provides these Janus $\text{MoSi}_2\text{N}_x\text{Z}_{4-x}$ metals a very competitive property among other 2D materials.

It is found that the piezoelectric effect can be generated by the electric polarization as well. The piezoelectricity is quantified by the coupling between polarization (P_i) and strain tensor (ϵ_{jk}), i.e., $e_{ijk} = \partial P_i / \partial \epsilon_{jk}$.^{37,39} The subscript i , j and k denote the x , y and

Table 1: OOP dipole moment (P_{out}), elastic coefficient (C_{11} and C_{12}) and OOP piezoelectric coefficients (e_{31} and d_{31}) of four polar metallic Janus $\text{MoSi}_2\text{N}_x\text{Z}_{4-x}$ monolayers.

Structure	P_{out}	e_{31}	C_{11}	C_{12}	d_{31}
	(pC/m)	(GPa)	(GPa)	(pm/V)	
MoSi_2N_4	*	*	537.18	159.70	*
MoSi_2P_4	*	*	171.16	61.93	*
MoSi_2As_4	*	*	126.90	42.74	*
$\text{MoSi}_2\text{N}_3\text{P}_1\text{-top}$	203	150	313.29	128.98	0.17
$\text{MoSi}_2\text{N}_1\text{As}_3\text{-mid}$	22	39	141.84	50.07	0.10
$\text{MoSi}_2\text{N}_2\text{P}_2\text{-4}$	24	101	176.97	104.79	0.18
$\text{MoSi}_2\text{N}_2\text{As}_2\text{-4}$	10	153	169.42	79.46	0.31

z direction. Here, we focus on the zigzag uniaxial strain effect on P_{out} , and investigate the OOP piezoelectric effect of these four Janus $\text{MoSi}_2\text{N}_x\text{Z}_{4-x}$ metals (Fig. S5). The linear fitting of P_{out} vs. uniaxial strain data determines the OOP piezoelectric strain coefficients (e_{31}) as 150 pC/m for $\text{MoSi}_2\text{N}_3\text{P}_1\text{-top}$, 39 pC/m for $\text{MoSi}_2\text{N}_1\text{As}_3\text{-mid}$, 101 pC/m of $\text{MoSi}_2\text{N}_2\text{P}_2\text{-4}$, and 153 pC/m for $\text{MoSi}_2\text{N}_2\text{As}_2\text{-4}$. These e_{31} values are quite larger than that of 1H-MoTe (50 pC/m,³⁶ half-metallic Co_2Se_3 (9 pC/m)³⁵ and Janus VSSe (98 pC/m),³⁷ and are comparable to e_{31} of InSe/TMDs van der Waals heterostructures (17–290 pC/m).³⁸

To further investigate the piezoelectric stress coefficients (d_{31}), it is necessary to get the deformation ability of the structures. 2D MoSi_2N_4 exhibits excellent mechanical properties as reported by previous experimental and theoretical studies.^{14,40} The elastic coefficients of MoSi_2X_4 decrease from $\text{X} = \text{N}$ to $\text{X} = \text{As}$ (Table 1), indicating N atoms play a crucial role in the rigidity of MA_2Z_4 family. When N atoms are replaced by P/As atoms, the rigidity of four $\text{MoSi}_2\text{N}_x\text{Z}_{4-x}$ metals is weaker than MoSi_2N_4 , implying that they are easily deformed. d_{31} of these four metals (with $3m$ point-group symmetry) can be defined as $d_{31} = e_{31}/(C_{11}+C_{12})$, where C_{11} and C_{12} are elastic constants.^{41,42} For $\text{MoSi}_2\text{N}_3\text{P}_1\text{-top}$, $\text{MoSi}_2\text{N}_1\text{As}_3\text{-mid}$, $\text{MoSi}_2\text{N}_2\text{P}_2\text{-4}$ and $\text{MoSi}_2\text{N}_2\text{As}_2\text{-4}$, d_{31} are 0.17, 0.10, 0.18 and 0.31 pV/m,

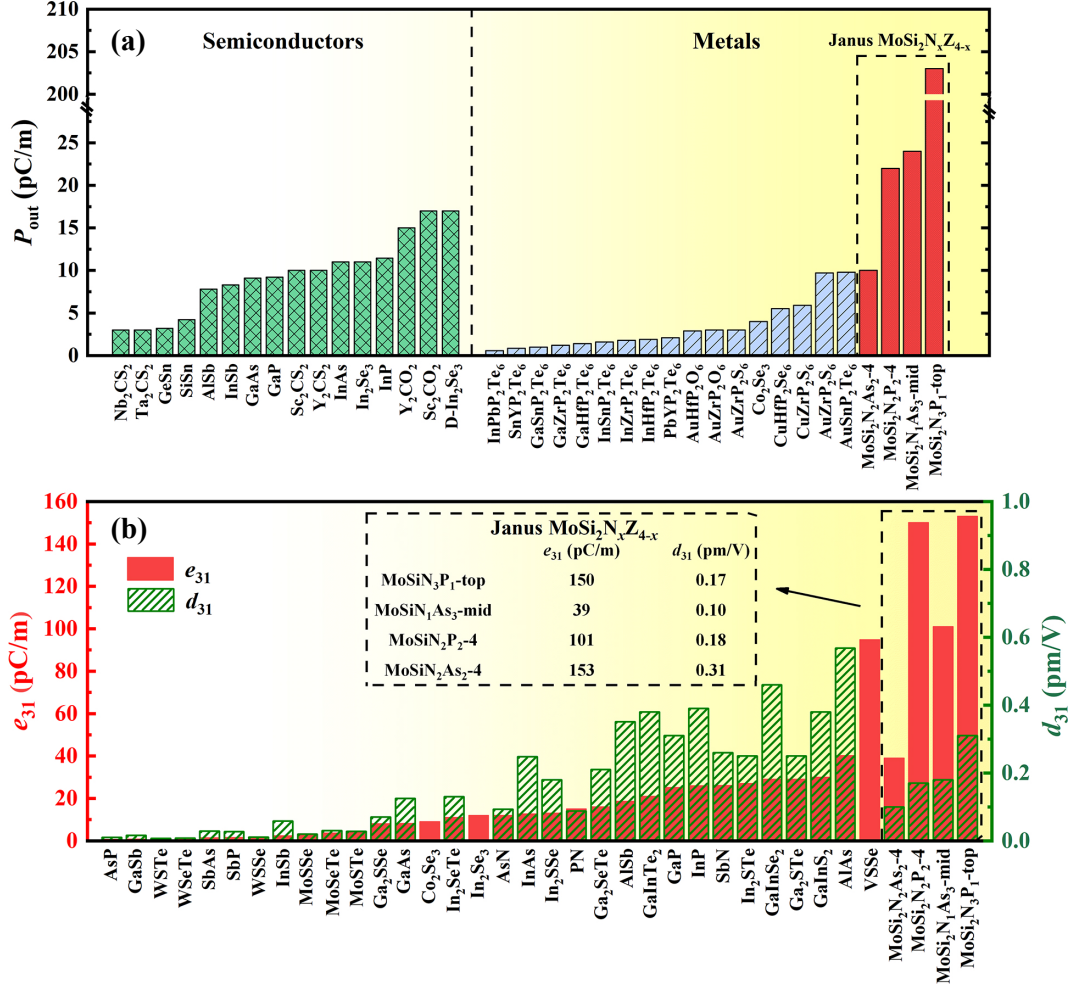


Figure 4: Comparison of (a) OOP polarization (P_{out}), (b) piezoelectric strain (e_{31}) and stress (d_{31}) coefficients between Janus metallic MoSi₂N_xZ_{4-x} monolayers and other 2D materials.^{13,32-38}

respectively. This OOP piezoelectricity d_{31} is comparable to the highest d_{31} that is reported so far for other 2D materials, as shown in Fig. 4(b).

3. CONCLUSIONS

In summary, we have reported polar and metallic Janus MoSi₂N_xZ_{4-x} (Z=P/As) monolayers that are derived from MoSi₂N₄ by breaking the OOP structural symmetry through Z substitution of N. Among the 13 stable MoSi₂N_xZ_{4-x} monolayers, there exist 6 semiconductors and 7 metals with four non-centrosymmetric Janus structures as polar metals. Although MoSi₂Z₄

(X=N/P/As) monolayers are semiconductors, these four Janus $\text{MoSi}_2\text{N}_x\text{Z}_{4-x}$ monolayers are found metallic. The metallic nature is originated from the 16th, 17th and 18th energy bands crossing Fermi level, which are mainly occupied by electrons from Mo- d orbitals. Analyzing charge density distribution and ELF reveal the conducting mechanism attributed to the delocalization of electrons around Mo atom. The non-centrosymmetric structure induces the asymmetric charge distribution along the OOP direction and thus the OOP electric polarization and piezoelectricity in four Janus metallic $\text{MoSi}_2\text{N}_x\text{Z}_{4-x}$ monolayers. P_{out} , e_{31} , and d_{31} are found up to 10–203 pC/m, 39–153 pC/m, and 0.10–0.31 pV/m, respectively, which are comparable to or even higher than the highest values that are reported so far for other 2D materials. These results demonstrate MoSi_2N_4 derived Janus monolayers as polar metals with large OOP piezoelectricity, enrich the 2D polar metal family with coexisting unusual properties, and could inspire the asymmetric structure design of polar metals with large piezoelectricity.

4. COMPUTATIONAL METHODS

First-principles calculations are performed by using Vienna *ab initio* Simulation Package (VASP) based on density functional theory (DFT).^{43,44} The electron-ion interactions and exchange-correlation function are described by the projector augmented wave (PAW) method⁴⁵ and the generalized gradient approximation (GGA) with Perdew–Burke–Ernzerhof (PBE),⁴⁶ respectively. For the confirmation of electric properties, e.g., band structures and semiconductor or metallic nature, the hybrid functional (HSE06)^{47,48} is utilized. The cutoff energy of plane wave is set as 500 eV. The convergence criteria for energy and force are 10^{-7} eV and 10^{-4} eV/Å, respectively. Monkhorst-Park k -mesh of a $21 \times 21 \times 1$ for unit cell in the first Brillouin zone is used. The vacuum region is set as 20 Å to eliminate the interactions between layers. In MoSi_2X_4 (X=N/P/As) and $\text{MoSi}_2\text{N}_x\text{Z}_{4-x}$ monolayers, the valence electron configurations are treated as $5s^24d^4$ for Mo, $3s^23p^2$ for Si, $2s^22p^3$ for N, $3s^23p^3$ for P and

$4s^24p^3$ for As. The structural stability is confirmed in terms of formation energy and lattice dynamics. The phonon dispersion spectra are obtained by the PHONOPY package with the finite displacement method.⁴⁹ The $5 \times 5 \times 1$ supercells and $5 \times 5 \times 1$ k -meshes are used the calculation of harmonic interatomic force constants (2^{nd} IFCs).

The formation energy (E_F) of $\text{MoSi}_2\text{N}_x\text{Z}_{4-x}$ is expressed as

$$E_F = \frac{E_{\text{MoSi}_2\text{N}_x\text{Z}_{4-x}} - (E_{\text{Mo}} + 2E_{\text{Si}} + xE_{\text{N}} + (4-x)E_{\text{Z}})}{N_{\text{atom}}} \quad (1)$$

where E_{Mo} , E_{Si} , E_{N} and E_{Z} are energy of isolated Mo, Si, N and Z atom, respectively. $E_{\text{MoSi}_2\text{N}_x\text{Z}_{4-x}}$ is the energy of $\text{MoSi}_2\text{N}_x\text{Z}_{4-x}$. N_{atom} is the number of total atoms.

Since the Berry phase method is problematic for calculating polarizations of metals,^{50,51} we utilize an alternative method based on classical electrodynamics. In the case that the vacuum slab is large enough to eliminate the interlayer interactions and neglect the periodicity, the out-of-plane polarization (P_{out}) can be easily defined by the classical electrodynamics and estimated as $P = q \times d$, where q is the total number of valence charge and d is the vector of dipole moment from negative center (NCC) to positive center (PCC).^{32,34,35} The z coordinates of NCC and PCC can be calculated as:

$$\text{NCC} = \frac{\int \int \int \rho z dx dy dz}{q} \quad (2)$$

$$\text{PCC} = \frac{\sum n z}{q} \quad (3)$$

in which ρ , z and n are the charge density, coordinate along the OOP z direction and valence electrons of each ion, respectively. The calculated P_{out} of monolayer $\alpha\text{-In}_2\text{Se}_3$ is 0.15 eÅ/u.c (18 pC/m), agreeing well with the previous measurements and theoretical calculations (0.095–0.18 eÅ/u.c).^{32,34,35,38,52} P_{out} of $\text{CrSe}_2\text{-1H}$ is calculated as 0.45 eÅ/u.c., in agreement with the calculation result (0.37 eÅ/u.c) as well.⁵³ These testing calculations validate the applicability of this method.

Supporting information

Supplementary material associated with this article can be found in the online version.

Acknowledgment

The authors acknowledge the support from the National Natural Science Foundation of China (NSFC 12272173, 11902150), 15th Thousand Youth Talents Program of China, the Research Fund of State Key Laboratory of Mechanics and Control for Aerospace Structures (MCMS-I-0419G01 and MCMS-I-0421K01), the Fundamental Research Funds for the Central Universities (1001-XAC21021), and a project Funded by the Priority Academic Program Development of Jiangsu Higher Education Institutions. This work is partially supported by High Performance Computing Platform of Nanjing University of Aeronautics and Astronautics. Simulations were also performed on Hefei advanced computing center.

References

- (1) Shi, Y. et al. A ferroelectric-like structural transition in a metal. Nature Materials **2013**, 12, 1024–1027.
- (2) Puggioni, D.; Rondinelli, J. M. Designing a robustly metallic noncentrosymmetric ruthenate oxide with large thermopower anisotropy. Nature Communications **2014**, 5, 3432.
- (3) Kim, T. H. et al. Polar metals by geometric design. Nature **2016**, 533, 68–72.
- (4) Benedek, N. A.; Birol, T. 'Ferroelectric' metals reexamined: Fundamental mechanisms and design considerations for new materials. Journal of Materials Chemistry C **2016**, 4, 4000–4015.

- (5) Cao, Y. et al. Artificial two-dimensional polar metal at room temperature. Nature Communications **2018**, 9, 1547.
- (6) Laurita, N. J.; Ron, A.; Shan, J. Y.; Puggioni, D.; Koocher, N. Z.; Yamaura, K.; Shi, Y.; Rondinelli, J. M.; Hsieh, D. Evidence for the weakly coupled electron mechanism in an Anderson-Blount polar metal. Nature Communications **2019**, 10, 3217.
- (7) Meng, M.; Wang, Z.; Fathima, A.; Ghosh, S.; Saghayezhian, M.; Taylor, J.; Jin, R.; Zhu, Y.; Pantelides, S. T.; Zhang, J.; Plummer, E. W.; Guo, H. Interface-induced magnetic polar metal phase in complex oxides. Nature Communications **2019**, 10, 5248.
- (8) Cai, W.; He, J.; Li, H.; Zhang, R.; Zhang, D.; Chung, D. Y.; Bhowmick, T.; Wolverton, C.; Kanatzidis, M. G.; Deemyad, S. Pressure-induced ferroelectric-like transition creates a polar metal in defect antiperovskites $\text{Hg}_3\text{Te}_2\text{X}_2$ ($\text{X} = \text{Cl}, \text{Br}$). Nature Communications **2021**, 12, 1509.
- (9) Ke, C.; Huang, J.; Liu, S. Two-dimensional ferroelectric metal for electrocatalysis. Materials Horizons **2021**, 8, 3387–3393.
- (10) Duan, X.; Huang, J.; Xu, B.; Liu, S. A two-dimensional multiferroic metal with voltage-tunable magnetization and metallicity. Materials Horizons **2021**, 8, 2316–2324.
- (11) Zhou, W. X. et al. Artificial two-dimensional polar metal by charge transfer to a ferroelectric insulator. Communications Physics **2019**, 2, 125.
- (12) Fei, Z.; Zhao, W.; Palomaki, T. A.; Sun, B.; Miller, M. K.; Zhao, Z.; Yan, J.; Xu, X.; Cobden, D. H. Ferroelectric switching of a two-dimensional metal. Nature **2018**, 560, 336–339.
- (13) Ma, X. Y.; Lyu, H. Y.; Hao, K. R.; Zhao, Y. M.; Qian, X.; Yan, Q. B.; Su, G. Large family of two-dimensional ferroelectric metals discovered via machine learning. Science Bulletin **2021**, 66, 233–242.

- (14) Hong, Y. L.; Liu, Z.; Wang, L.; Zhou, T.; Ma, W.; Xu, C.; Feng, S.; Chen, L.; Chen, M. L.; Sun, D. M.; Chen, X. Q.; Cheng, H. M.; Ren, W. Chemical vapor deposition of layered two-dimensional MoSi_2N_4 materials. Science **2020**, 369, 670–674.
- (15) Wang, L.; Shi, Y.; Liu, M.; Zhang, A.; Hong, Y. L.; Li, R.; Gao, Q.; Chen, M.; Ren, W.; Cheng, H. M.; Li, Y.; Chen, X. Q. Intercalated architecture of MA_2Z_4 family layered van der Waals materials with emerging topological, magnetic and superconducting properties. Nature Communications **2021**, 12, 2361.
- (16) Cao, L.; Zhou, G.; Wang, Q.; Ang, L. K.; Ang, Y. S. Two-dimensional van der Waals electrical contact to monolayer MoSi_2N_4 . Applied Physics Letters **2021**, 118, 013106.
- (17) Yang, J. S.; Zhao, L.; Li, S. Q.; Liu, H.; Wang, L.; Chen, M.; Gao, J.; Zhao, J. Accurate electronic properties and non-linear optical response of two-dimensional MA_2Z_4 . Nanoscale **2021**, 13, 5479–5488.
- (18) Yao, H.; Zhang, C.; Wang, Q.; Li, J.; Yu, Y.; Xu, F.; Wang, B.; Wei, Y. Novel two-dimensional layered MoSi_2Z_4 ($\text{Z} = \text{P}, \text{As}$): New promising optoelectronic materials. Nanomaterials **2021**, 11, 559.
- (19) Huang, D.; Liang, F.; Guo, R.; Lu, D.; Wang, J.; Yu, H.; Zhang, H. MoSi_2N_4 : A 2D regime with strong exciton-phonon coupling. Advanced Optical Materials **2022**, 10, 2102612.
- (20) Zhong, T.; Ren, Y.; Zhang, Z.; Gao, J.; Wu, M. Sliding ferroelectricity in two-dimensional MoA_2N_4 ($\text{A} = \text{Si}$ or Ge) bilayers: high polarizations and Moiré potentials. Journal of Materials Chemistry A **2021**, 9, 19659–19663.
- (21) Yu, J.; Zhou, J.; Wan, X.; Li, Q. High intrinsic lattice thermal conductivity in monolayer MoSi_2N_4 . New Journal of Physics **2021**, 23, 033005.

- (22) Yin, Y.; Yi, M.; Guo, W. High and anomalous thermal conductivity in monolayer MSi_2Z_4 semiconductors . ACS Applied Materials & Interfaces **2021**, 13, 45907–45915.
- (23) Li, S.; Wu, W.; Feng, X.; Guan, S.; Feng, W.; Yao, Y.; Yang, S. A. Valley-dependent properties of monolayer MoSi_2N_4 , WSi_2N_4 , and MoSi_2As_4 . Physical Review B **2020**, 102, 235435.
- (24) Chen, J.; Tang, Q. The versatile electronic, magnetic and photo-electro catalytic activity of a new 2D MA_2Z_4 family. Chemistry - A European Journal **2021**, 27, 9925–9933.
- (25) Li, Y.; Wang, J.; Yang, G.; Liu, Y. Strain-induced magnetism in MSi_2N_4 ($\text{M} = \text{V}, \text{Cr}$): A first-principles study. Annalen der Physik **2021**, 533, 2100273.
- (26) Akanda, M. R. K.; Lake, R. K. Magnetic properties of NbSi_2N_4 , VSi_2N_4 , and VSi_2P_4 monolayers. Applied Physics Letters **2021**, 119, 052402.
- (27) Yin, Y.; Gong, Q.; Yi, M.; Guo, W. Emerging versatile two-dimensional MoSi_2N_4 family. arXiv **2022**, arXiv:2211.00827.
- (28) Zhou, W.; Wu, L.; Li, A.; Zhang, B.; Ouyang, F. Structural symmetry, spin-orbit coupling, and valley-related properties of monolayer WSi_2N_4 family. Journal of Physical Chemistry Letters **2021**, 12, 11622–11628.
- (29) Guo, S. D.; Mu, W. Q.; Zhu, Y. T.; Han, R. Y.; Ren, W. C. Predicted septuple-atomic-layer Janus MSiGeN_4 ($\text{M} = \text{Mo}$ and W) monolayers with Rashba spin splitting and high electron carrier mobilities. Journal of Materials Chemistry C **2021**, 9, 2464–2473.
- (30) Ding, Y.; Wang, Y. First-principles study of two-dimensional $\text{MoN}_2\text{X}_2\text{Y}_2$ ($\text{X}=\text{B-In}$, $\text{Y}=\text{N-Te}$) nanosheets: The III-VI analogues of MoSi_2N_4 with peculiar electronic and magnetic properties. Applied Surface Science **2022**, 593, 153317.
- (31) Zhang, S.; Wang, Q.; Kawazoe, Y.; Jena, P. Three-dimensional metallic boron nitride. Journal of the American Chemical Society **2013**, 135, 18216–18221.

- (32) Zhang, L.; Tang, C.; Zhang, C.; Du, A. First-principles screening of novel ferroelectric MXene phases with a large piezoelectric response and unusual auxeticity. Nanoscale **2020**, 12, 21291–21298.
- (33) Di Sante, D.; Stroppa, A.; Barone, P.; Whangbo, M. H.; Picozzi, S. Emergence of ferroelectricity and spin-valley properties in two-dimensional honeycomb binary compounds. Physical Review B - Condensed Matter and Materials Physics **2015**, 91, 161401.
- (34) Tang, C.; Zhang, L.; Wijethunge, D.; Ostrikov, K. K.; Du, A. Controllable Polarization and Doping in Ferroelectric In_2Se_3 Monolayers and Heterobilayers via Intrinsic Defect Engineering. Journal of Physical Chemistry C **2021**, 125, 24648–24654.
- (35) Tang, C.; Zhang, L.; Jiao, Y.; Zhang, C.; Sanvito, S.; Du, A. First-principles prediction of polar half-metallicity and out-of-plane piezoelectricity in two-dimensional quintuple layered cobalt selenide. Journal of Materials Chemistry C **2021**, 9, 12046–12050.
- (36) Yagmurcukardes, M.; Sevik, C.; Peeters, F. M. Electronic, vibrational, elastic, and piezoelectric properties of monolayer Janus MoSTe phases: A first-principles study. Physical Review B **2019**, 100, 045415.
- (37) Zhang, C.; Nie, Y.; Sanvito, S.; Du, A. First-principles prediction of a room-temperature ferromagnetic Janus VSSe monolayer with piezoelectricity, ferroelasticity, and large valley polarization. Nano Letters **2019**, 19, 1366–1370.
- (38) Chen, Y.; Tang, Z.; Shan, H.; Jiang, B.; Ding, Y.; Luo, X.; Zheng, Y. Enhanced out-of-plane piezoelectric effect in In_2Se_3 /transition metal dichalcogenide heterostructures. Physical Review B **2021**, 104, 075449.
- (39) Wu, W.; Wang, L.; Li, Y.; Zhang, F.; Lin, L.; Niu, S.; Chenet, D.; Zhang, X.; Hao, Y.; Heinz, T. F.; Hone, J.; Wang, Z. L. Piezoelectricity of single-atomic-layer MoS_2 for energy conversion and piezotronics. Nature **2014**, 514, 470–474.

- (40) Li, Q.; Zhou, W.; Wan, X.; Zhou, J. Strain effects on monolayer MoSi₂N₄: Ideal strength and failure mechanism. Physica E: Low-Dimensional Systems and Nanostructures **2021**, 131, 114753.
- (41) Fei, R.; Li, W.; Li, J.; Yang, L. Giant piezoelectricity of monolayer group IV monochalcogenides: SnSe, SnS, GeSe, and GeS. Applied Physics Letters **2015**, 107, 173104.
- (42) Yin, H.; Gao, J.; Zheng, G. P.; Wang, Y.; Ma, Y. Giant piezoelectric effects in monolayer group-V binary compounds with honeycomb phases: A first-principles prediction. Journal of Physical Chemistry C **2017**, 121, 25576–25584.
- (43) Hafner, J. Materials simulations using VASP—a quantum perspective to materials science. Computer Physics Communications **2007**, 177, 6–13.
- (44) Hafner, J. Ab-initio simulations of materials using VASP: Density-functional theory and beyond. Journal of computational chemistry **2008**, 29, 2044–2078.
- (45) Blöchl, P. E. Projector augmented-wave method. Physical Review B **1994**, 50, 17953–17979.
- (46) Perdew, J. P.; Burke, K.; Ernzerhof, M. Generalized gradient approximation made simple. Physical Review Letters **1996**, 77, 3865–3868.
- (47) Vydrov, O. A.; Heyd, J.; Krukau, A. V.; Scuseria, G. E. Importance of short-range versus long-range Hartree-Fock exchange for the performance of hybrid density functionals. Journal of Chemical Physics **2006**, 125, 074106.
- (48) Paier, J.; Marsman, M.; Hummer, K.; Kresse, G.; Gerber, I. C.; Ángyán, J. G. Screened hybrid density functionals applied to solids. Journal of Chemical Physics **2006**, 124, 154709.

- (49) Togo, A.; Tanaka, I. First principles phonon calculations in materials science. Scripta Materialia **2015**, 108, 1–5.
- (50) Resta, R. Why are insulators insulating and metals conducting? Journal of Physics Condensed Matter **2002**, 14, R625–R656.
- (51) Xu, T.; Zhang, J.; Zhu, Y.; Wang, J.; Shimada, T.; Kitamura, T.; Zhang, T. Y. Two-dimensional polar metal of a PbTe monolayer by electrostatic doping. Nanoscale Horizons **2020**, 5, 1400–1406.
- (52) Ding, W.; Zhu, J.; Wang, Z.; Gao, Y.; Xiao, D.; Gu, Y.; Zhang, Z.; Zhu, W. Prediction of intrinsic two-dimensional ferroelectrics in In_2Se_3 and other $\text{III}_2\text{-VI}_3$ van der Waals materials. Nature Communications **2017**, 8, 14956.
- (53) Li, Y.; Legut, D.; Liu, X.; Lin, C.; Feng, X.; Li, Z.; Zhang, Q. Modulated ferromagnetism and electric polarization induced by surface vacancy in MX_2 monolayers. Journal of Physical Chemistry C **2022**, 126, 8817–8825.

Monolayer polar metals with large piezoelectricity derived from MoSi_2N_4

Yan Yin,[†] Qihua Gong,^{*,†,‡} and Min Yi^{*,†}

[†]*State Key Laboratory of Mechanics and Control for Aerospace Structures & Key Laboratory for Intelligent Nano Materials and Devices of Ministry of Education & Institute for Frontier Science & College of Aerospace Engineering, Nanjing University of Aeronautics and Astronautics (NUAA), Nanjing 210016, China*

[‡]*MIIT Key Laboratory of Aerospace Information Materials and Physics & College of Physics, Nanjing University of Aeronautics and Astronautics (NUAA), Nanjing 211106, China*

E-mail: gongqihua@nuaa.edu.cn; yimin@nuaa.edu.cn

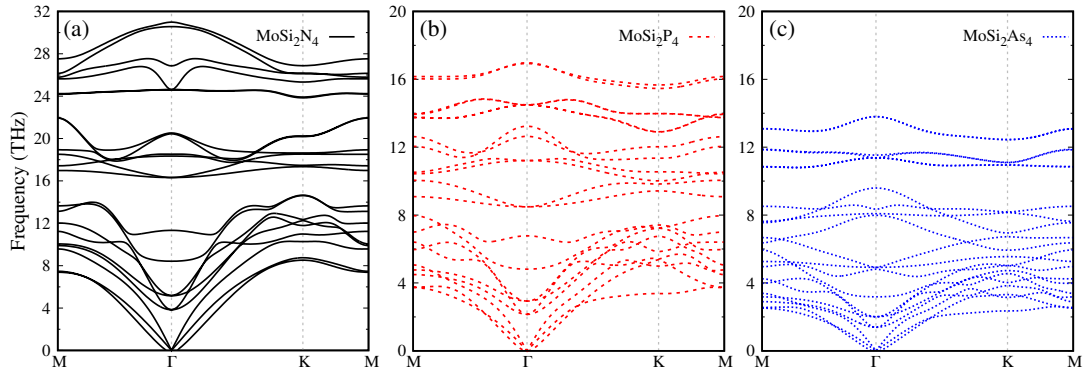


Fig. S1. Phonon dispersion spectra of (a) MoSi_2N_4 , (b) MoSi_2P_4 and (c) MoSi_2As_4 .

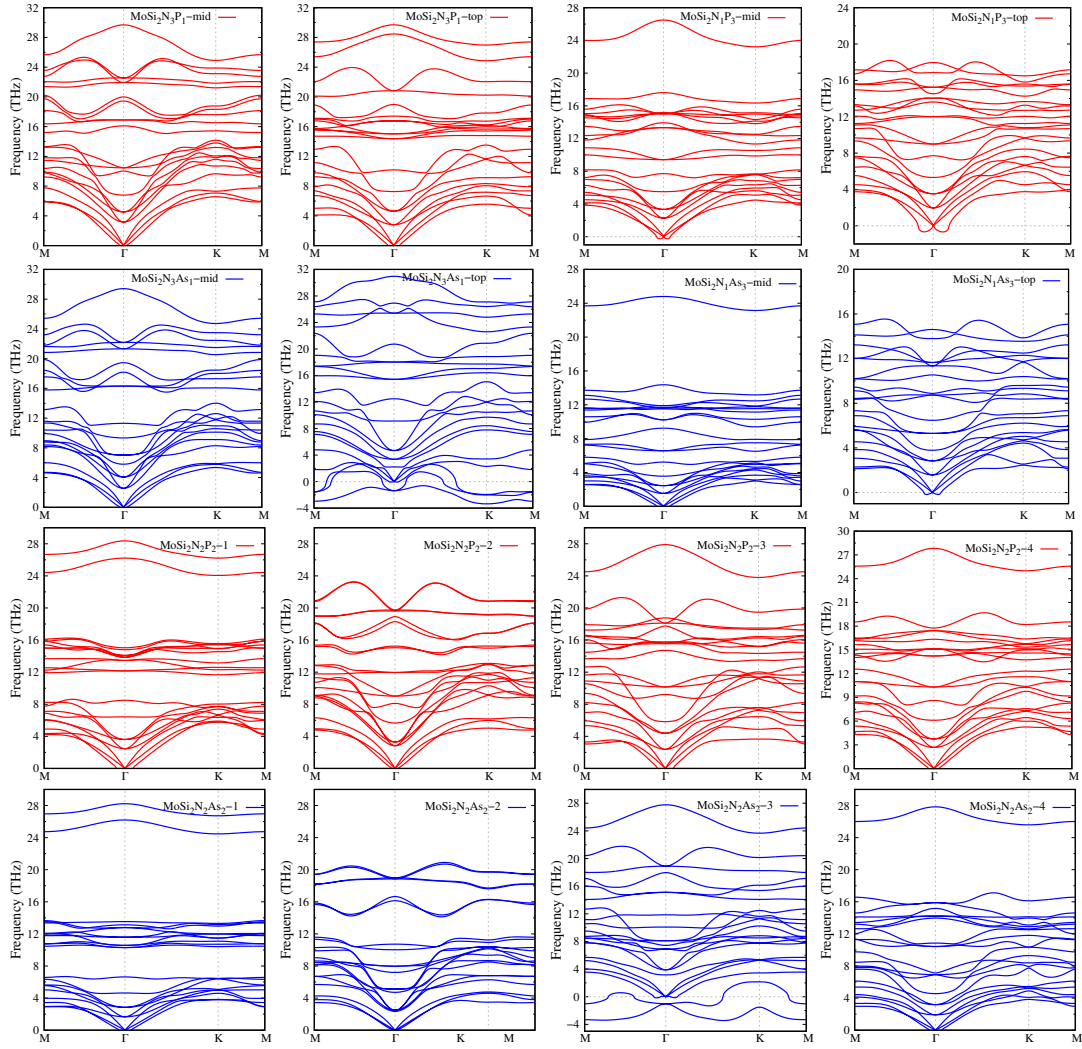


Fig. S2. Phonon dispersion spectra of $\text{MoSi}_2\text{N}_x\text{Z}_{4-x}$ monolayers.

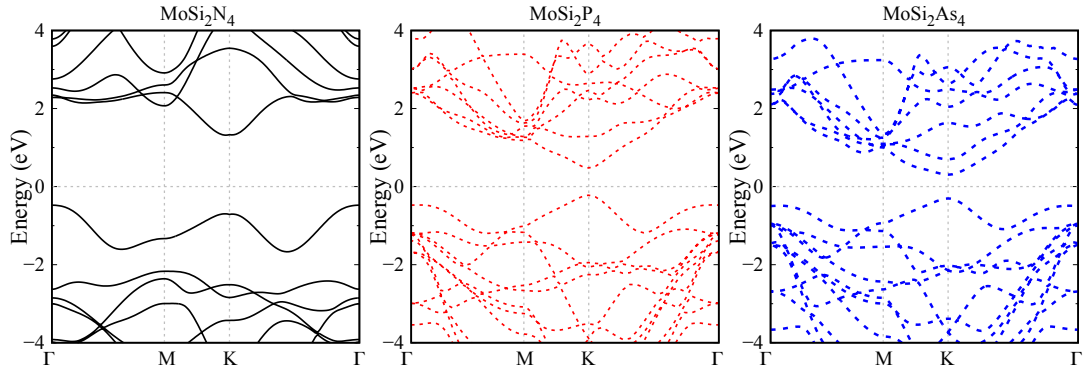


Fig. S3. Band structures of MoSi_2X_4 ($\text{X}=\text{N}/\text{P}/\text{As}$).

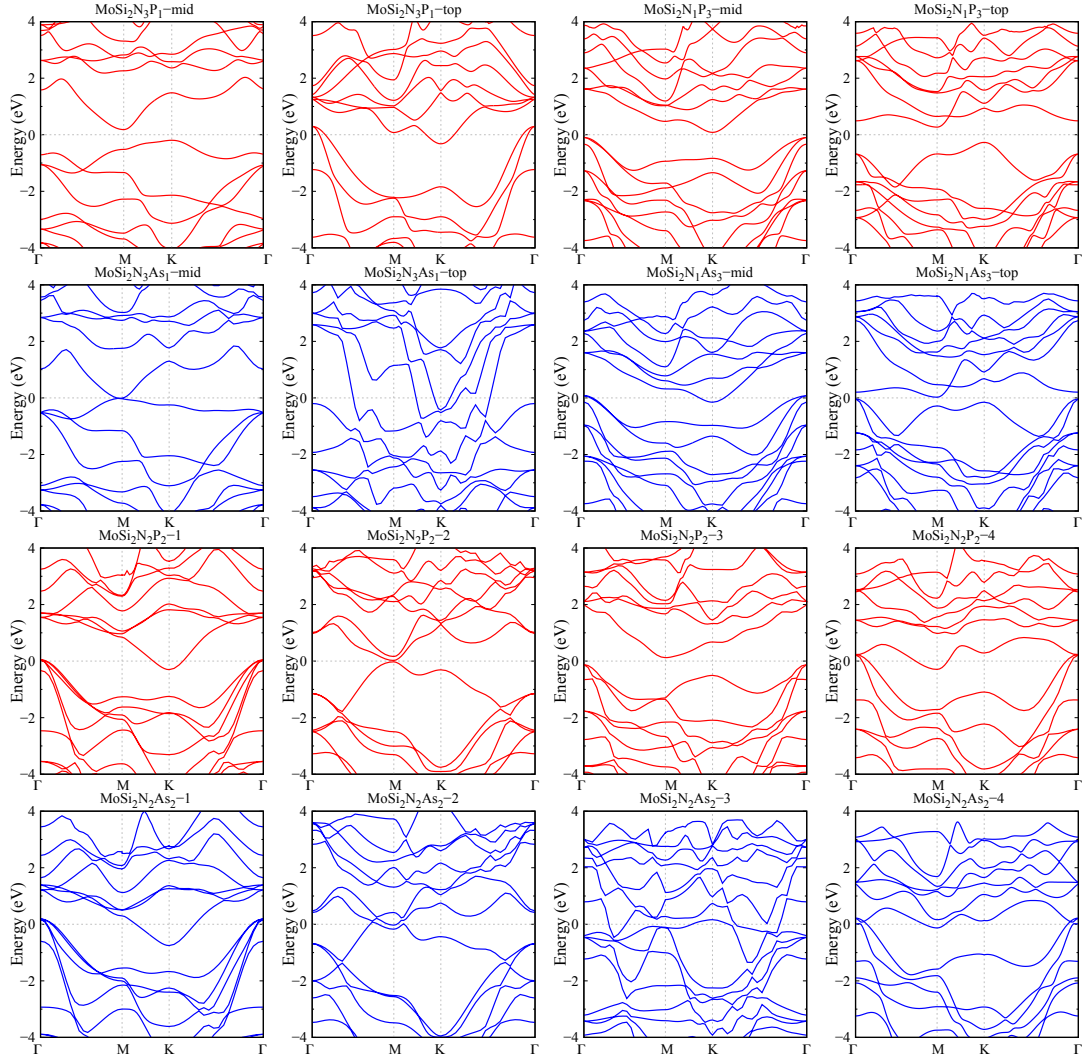


Fig. S4. Band structures of $\text{MoSi}_2\text{N}_x\text{Z}_{4-x}$ monolayers.

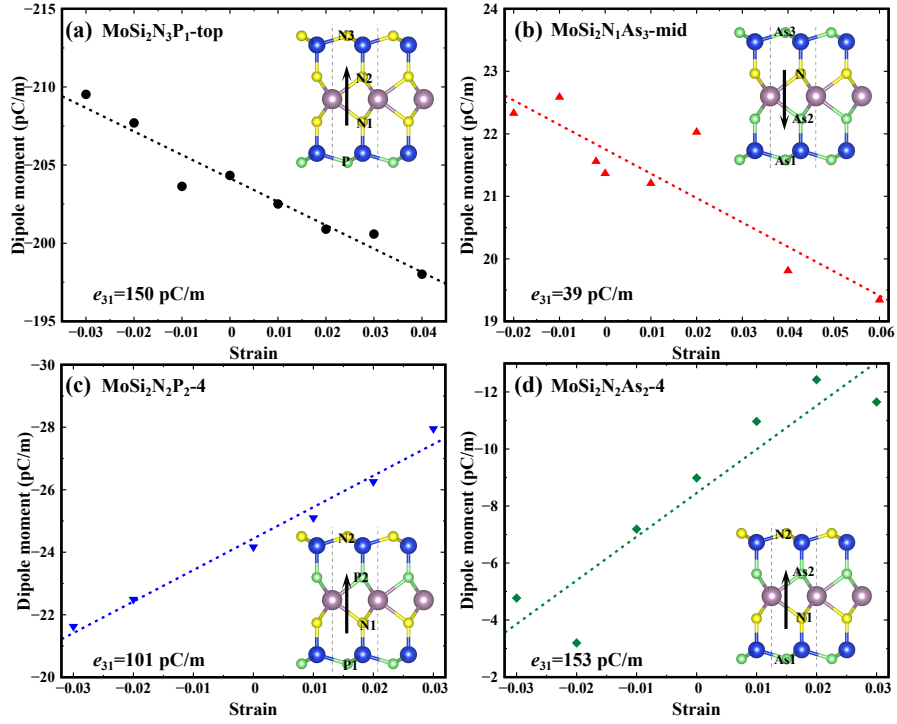


Fig. S5. OOP dipole moment as a function of zigzag uniaxial strain: (a) $\text{MoSi}_2\text{N}_3\text{P}_1\text{-top}$, (b) $\text{MoSi}_2\text{N}_1\text{As}_3\text{-mid}$, (c) $\text{MoSi}_2\text{N}_2\text{P}_2\text{-4}$, (d) $\text{MoSi}_2\text{N}_2\text{As}_2\text{-4}$. The inset arrows indicate the dipole moment direction.

Table S1. Structural parameters of $\text{MoSi}_2\text{N}_x\text{Z}_{4-x}$ monolayers, i.e., lattice constants, thickness (h), bond length, formation energy (E_f), dynamical stability and band gap from PBE (E_g^{PBE}) and HSE (E_g^{HSE})

Structure	$a = b$	h	$d_{\text{Z4-Si2}}$	$d_{\text{Z3-Si2}}$	$d_{\text{Z3-Mo}}$	$d_{\text{Z2-Mo}}$	$d_{\text{Z2-Si1}}$	$d_{\text{Z1-Si1}}$	E_F	Dynamics	E_g^{PBE}	E_g^{HSE}
	(Å)	(Å)	(Å)	(Å)	(Å)	(Å)	(Å)	(Å)	(eV/atom)	(Y/N)	(eV)	(eV)
MoSi_2N_4	2.91	10.01	1.76	1.75	2.10	2.10	1.75	1.76	-0.94	Y	1.79	*
MoSi_2P_4	3.47	13.17	2.25	2.24	2.46	2.46	2.24	2.25	-0.34	Y	0.70	*
MoSi_2As_4	3.62	13.94	2.37	2.36	2.56	2.56	2.36	2.37	-0.09	Y	0.56	*
$\text{MoSi}_2\text{N}_3\text{P}_1$ -mid	2.98	10.92	1.79	2.23	2.37	2.12	1.75	1.79	-0.28	Y	0.38	0.96
$\text{MoSi}_2\text{N}_3\text{P}_1$ -top	3.05	10.95	2.15	1.73	2.14	2.13	1.75	1.82	-0.49	Y	*	*
$\text{MoSi}_2\text{N}_2\text{P}_2$ -1	3.23	11.71	2.18	1.75	2.21	2.21	1.75	2.18	-0.24	Y	*	*
$\text{MoSi}_2\text{N}_2\text{P}_2$ -2	3.05	11.72	1.83	2.23	2.38	2.38	2.23	1.83	-0.53	Y	0.05	0.63
$\text{MoSi}_2\text{N}_2\text{P}_2$ -3	3.14	11.66	1.87	1.76	2.16	2.39	2.23	2.16	-0.39	Y	0.24	0.88
$\text{MoSi}_2\text{N}_2\text{P}_2$ -4	3.15	11.67	1.86	2.25	2.39	2.17	1.73	2.17	-0.37	Y	*	*
$\text{MoSi}_2\text{N}_1\text{P}_3$ -mid	3.33	12.34	2.20	1.75	2.23	2.42	2.24	2.21	-0.27	Y	0.18	0.40
$\text{MoSi}_2\text{N}_1\text{P}_3$ -top	3.26	12.33	1.93	2.24	2.42	2.42	2.23	2.19	-1.35	N	0.54	0.58
$\text{MoSi}_2\text{N}_3\text{As}_1$ -mid	2.99	11.15	1.80	2.35	2.47	2.12	1.75	1.79	-0.56	Y	0.01	0.48
$\text{MoSi}_2\text{N}_3\text{As}_1$ -top	2.88	12.63	1.74	1.74	2.09	2.09	1.78	3.13	-0.46	N	*	*
$\text{MoSi}_2\text{N}_2\text{As}_2$ -1	3.31	12.05	2.30	1.73	2.23	2.23	1.733	2.30	-0.04	Y	*	*
$\text{MoSi}_2\text{N}_2\text{As}_2$ -2	3.08	12.21	1.83	2.36	2.48	2.48	2.36	1.83	-0.28	Y	*	*
$\text{MoSi}_2\text{N}_2\text{As}_2$ -3	3.11	12.42	1.85	1.75	2.14	2.49	2.37	2.38	0.21	N	*	*
$\text{MoSi}_2\text{N}_2\text{As}_2$ -4	3.20	12.04	1.89	2.38	2.49	2.18	1.71	2.29	-0.14	Y	*	*
$\text{MoSi}_2\text{N}_1\text{As}_3$ -mid	3.49	12.77	2.34	1.74	2.27	2.54	2.36	2.33	-0.05	Y	*	*
$\text{MoSi}_2\text{N}_1\text{As}_3$ -top	3.35	12.88	1.97	2.37	2.49	2.51	2.34	2.30	-0.03	Y	0.04	0.52